

# Emulsification in a microfluidic flow-focusing device: effect of the viscosities of the liquids

Zhihong Nie · MinsSeok Seo · Shengqing Xu · Patrick C. Lewis · Michelle Mok · Eugenia Kumacheva · George M. Whitesides · Piotr Garstecki · Howard A. Stone

Received: 6 July 2007 / Accepted: 13 February 2008 / Published online: 6 March 2008  
© Springer-Verlag 2008

**Abstract** We report the results of a comparative study of microfluidic emulsification of liquids with different viscosities. Depending on the properties of the fluids and their rates of flow, emulsification occurred in the dripping and jetting regimes. We studied the characteristic features and typical dependence of the size and of the size distribution of droplets in each regime. For each liquid, we identified a range of hydrodynamic conditions promoting generation of highly monodisperse droplets. Viscosity played an

important role in emulsification: highly viscous liquids were emulsified into larger droplets with lower polydispersity. Although it was not possible to provide a unified scaling for the volumes of the droplets, our results suggest that the break-up dynamics of the lower viscosity fluids resembles the rate-of-flow-controlled break-up, as reported earlier for the formation of bubbles in flow-focusing geometries [Garstecki P, Stone HA, Whitesides GM (2005) *Phys Rev Lett* 94:164501]. The results of this study can be helpful for a rationalized selection of liquids for the controlled formation of droplets with a predetermined size and with a narrow distribution of sizes.

Z. Nie · M. Seo · S. Xu · P. C. Lewis · E. Kumacheva (✉)  
Department of Chemistry, University of Toronto,  
80 St. George Street, Toronto, ON, Canada M5S 3H6  
e-mail: ekumache@alchemy.chem.utoronto.ca;  
ekumache@chem.utoronto.ca

M. Mok · E. Kumacheva  
Department of Chemical Engineering and Applied Chemistry,  
University of Toronto, 200 College street,  
Toronto, ON, Canada M5S 3E5

E. Kumacheva  
Institute of Biomaterials and Biomedical Engineering,  
University of Toronto, 4 Taddle Creek Road,  
Toronto, ON, Canada

G. M. Whitesides  
Department of Chemistry and Chemical Biology,  
Harvard University, 12 Oxford St., Cambridge,  
MA 02138-4307, USA

P. Garstecki  
Institute of Physical Chemistry, Polish Academy of Sciences,  
Kasprzaka 44/52, 01-224 Warsaw, Poland

H. A. Stone  
School of Engineering and Applied Sciences,  
Harvard University, Cambridge, MA 02138-4307, USA

**Keywords** Microfluidic · Hydrodynamic · Droplets · Flow-focusing · Emulsification

## 1 Introduction

Recently, several research groups have reported synthesis of polymer particles in microfluidic reactors (Cohen et al. 2001; Dendukuri et al. 2005; Jeong et al. 2005; Lewis et al. 2005; Loscertales et al. 2002; Nie et al. 2005, 2006; Nisisako et al. 2004; Seo et al. 2005a, 2005b; Takeuchi et al. 2005; Utada et al. 2005; Xu et al. 2005; Zhang et al. 2006). The syntheses included a two-step process: (1) microfluidic emulsification of monomer or polymeric fluids, and (2) subsequent in-situ (on chip) solidification of the droplets by means of polymerization, gelation, or solvent evaporation. Microfluidic methods allowed for the production of particles with diameters from several micrometers to hundreds of micrometers, polydispersities below 5%, and shapes and morphologies that were not achievable in the conventional synthesis of colloids (Nisisako et al. 2004; Xu et al. 2005; Nie et al. 2005, 2006;

Dendukuri et al. 2005). Such particles have a broad range of potential applications including their use as ion exchange resins, spacers, calibration standards, and carriers for drugs, nutrition, pharmaceutical, and cosmetics agents.

Most commonly used microemulsification devices include T-junctions (Christopher and Anna 2007; Dreyfus et al. 2003; Link et al. 2004; Nisisako et al. 2002; Thorsen et al. 2001; Garstecki et al. 2006), flow-focusing devices (Anna et al. 2003; Ganan-Calvo 1998; Ganan-Calvo and Gordillo 2001; Xu and Nakajima 2004; Garstecki et al. 2004), and devices in which liquid threads break on the terraces of microchannels (Sugiura et al. 2001, 2002a, b). Since the generation of droplets with a predictable and reproducible size and size distribution determines their potential applications (including the synthesis of polymer colloids), several research groups have explored various aspects of the process of emulsification (Seo et al. 2005a; Xu et al. 2005; Zhang et al. 2006; Cygan et al. 2005; El-Ali et al. 2005; Garstecki et al. 2005a; Hudson et al. 2005; Jensen and Lee 2004; Khan et al. 2004; Song et al. 2003; Zheng and Ismagilov 2005; Zheng et al. 2003). It has been observed that the size of droplets is controlled by the design of the microfluidic device (Sugiura et al. 2002a, b; Tan et al. 2006), the properties of liquids, and the rates of flow of two immiscible phases (Cramer et al. 2004; Ganan-Calvo 1998; Ganan-Calvo and Gordillo 2001; Garstecki et al. 2004, 2005a, 2005b, 2006; Thorsen et al. 2001; Serra et al. 2007; Tice et al. 2003; Ward et al. 2005).

Nevertheless, a detailed, quantitative, and generalized description of microemulsification of liquids with *varying* properties in the microconfined geometries of flow-focusing devices is still not available, although emulsification was extensively studied for many years in unbounded conditions. We note strong differences between the break-up of liquid threads in unbounded conditions (Cramer et al. 2004; Ganan-Calvo 1998; Utada et al. 2005; Serra et al. 2007; Zhang and Stone 1997) and in microconfined geometries (Anna et al. 2003; Garstecki et al. 2004, 2005b, 2005c, 2006; Thorsen et al. 2001). For example, Cramer et al. (2004) reported that in the case of break-up in co-flow of liquids in unbounded conditions a decrease in the value of interfacial tension between the immiscible phases results in the reduction of droplet size. In contrast, the dynamics of break-up of a low viscosity (compared to the viscosity of the continuous fluid) fluid in a microfluidic flow-focusing geometry was found to be largely independent of the value of interfacial tension, provided that the value of the capillary number ( $Ca$ , definition given below) was low enough (Garstecki et al. 2005c). Furthermore, a numerical study conducted by Zhang and Stone (Zhang and Stone 1997) for unbounded systems operating at low values of  $Ca$  showed that the volume of primary droplets depended only weakly on the ratio of viscosities of dispersed phase to continuous

phase. Cramer et al. (2004) reported similar observations in a co-flowing liquid–liquid system. In contrast, for microfluidic emulsification conducted at low values of  $Ca$ , Seo et al. (2005b) observed a strong effect of viscosity of the dispersed phase on the size of droplets produced from multifunctional monomers.

The goal of the present study was to systematically probe for the dependence of both qualitative and quantitative features of the operation of the microfluidic flow-focusing device (MFFD) on the viscosity of the dispersed phase, for which we use Newtonian fluids of viscosities ranging from 10 to 500 cP. On the basis of our results we discuss the dynamics of break-up in the context of relevant models, that is: (1) the shearing model, that relates the diameter of the droplet to the reciprocal of the capillary number, and (2) the rate-of-flow-controlled-breakup (or squeezing) model (Garstecki et al. 2005c, 2006; Guillot and Colin 2005), that relates the size of the droplet only to the ratio of the rates of flow of the dispersed and the continuous phase. From a practical point of view, our study provides guidelines for producing droplets with a predetermined size and polydispersity from liquids with well-defined macroscopic properties, using a MFFD.

## 2 Experimental

### 2.1 Materials

Monomers tripropyleneglycol diacrylate (TPGDA), dimethacrylate oxypropyldimethyl siloxane (MAOP-DMS), and divinyl benzene (DVB), and five samples of silicone oil with viscosity from 10 to 500 cP, were obtained from Aldrich Canada and used as received. These liquids were emulsified in an aqueous 2 wt% sodium dodecyle sulphate (SDS) solution. The viscosities of the liquids were measured at 25°C using either an Ubbelohde viscometer (viscometer constant  $K = 0.0999$ ), or Brookfield DV-III rheometer (MA, USA). The rheology measurements (TA Instruments, Inc. AR 2000 Rheometer) verified that all liquids studied in the present work showed Newtonian behavior. Interfacial tensions between the monomeric liquids or silicone oil and the SDS solution were measured by the axisymmetric droplet shape method (Freer et al. 2005) using the Kruss tensiometer (DSA100). Table 1 summarizes the properties of the liquids that we used in the present work.

### 2.2 Microfluidic flow-focusing device

We used soft-lithography (Xia and Whitesides 1998) to fabricate a MFFD in polyurethane elastomer. The elastomer was prepared by mixing a polyurethane intermediate (Airthane PET-60D, Air Products, USA) with 20 wt% of

**Table 1** Properties of emulsified liquids

Liquids	Density (g/cm <sup>3</sup> )	Dynamic viscosity $\eta$ (g · m <sup>-1</sup> · s <sup>-1</sup> , cP)	Interfacial tension <sup>a</sup> , $\gamma$ (mN/m)
TPGDA	1.03	14.0	2.8
MAOP-DMS	0.98	19.6	2.7
DVB	0.91	1.0	4.0
Silicone oil	0.93	10	3.3
Silicone oil	0.95	20	5.5
Silicone oil	0.96	50	4.8
Silicone oil	0.96	100	3.8
Silicone oil	0.97	500	4.9
2.0 wt% SDS aqueous solution	1.0	1.0	–

<sup>a</sup> Interfacial tension between the droplet phase and 2.0 wt% SDS aqueous solution

poly(ethylene glycol) (Sigma-Aldrich, USA) and 0.02 wt% of DABCO T-12 catalyst (Air Products, USA). The value of wetting angle of water on polyurethane was ca. 82°. The use of MFFD fabricated in polyurethane allowed for the production of oil-in-water emulsions (Seo et al. 2005b; Li et al. 2007). Masters were prepared using SU-8 photoresist (MicroChem, USA). Figure 1 shows a schematic of the MFFD (Anna et al. 2003). The device has an orifice with a width of 80 μm placed at a distance 250 μm downstream of three inlet streams. The height of the channels was 86 μm and the ratio of the height to the width of the orifice was ca. 1. A pressure gradient applied along the long axis of the MFFD forced the fluids into the orifice where the thread of the nonpolar liquid broke up in a periodic fashion to release droplets into the outlet channel. The aqueous phase was supplied from the two side channels and the droplet phase was supplied into the central channel.

The liquids were supplied to the MFFD via polyethylene (Intramedic, USA, PE60, I.D. 0.76 mm, O.D. 1.22 mm) or teflon tubing attached to syringes operated by two digitally-controlled syringe pumps (Harvard Apparatus, USA, PHD 2000 series). When the flow rate of liquids was changed,

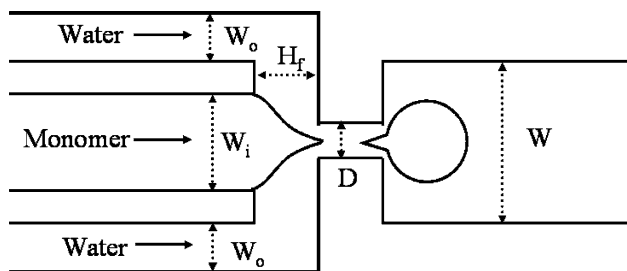


**Fig. 1** Schematic of flow-focusing microfluidic device. An orifice is placed at a distance  $H_f = 250 \mu\text{m}$  downstream of three coaxial inlet streams. Water is supplied to the two side channels which have widths  $W_o = 120 \mu\text{m}$ ; monomer is forced into the central channel which has a width  $W_i = 100 \mu\text{m}$ . The width of the orifice is  $D = 80 \mu\text{m}$ ; the width of the downstream channel is  $W = 240 \mu\text{m}$ . The height of the MFFD is  $86 \mu\text{m}$

the system was allowed to equilibrate for at least 3 min. We used an Olympus BX51 microscope and a high-speed camera (Photometrics CoolSNAR ES) to analyze the variation in the size of the droplets generated in the MFFD. The polydispersity of the droplets was characterized as the coefficient of variance (CV) as  $CV (\%) = (\sigma/D) \times 100$ , where  $\sigma$  is the standard deviation of droplet diameter (μm) and  $D$  is the mean diameter of the droplets (μm). To obtain  $D$  and CV of droplets, for each experimental point on the graphs we measured the dimensions of at least 500 droplets.

We studied the emulsification process in two types of experiments. We either varied the flow rate,  $Q_o$ , of the continuous phase, at a constant flow rate,  $Q_i$ , of the droplet phase, or generated droplets at a constant ratio of the two flow rates  $Q_o/Q_i$ , between the continuous and droplet phases, by simultaneously changing the flow rates of the two phases.

The ratio of the viscous stress to the stress imposed by interfacial tension between the liquids was accounted by the capillary number of the liquid as  $Ca = \eta v/\gamma$  where  $\eta$  and  $v$  are the dynamic viscosity and the mean velocity of the liquid, respectively ( $v$  was determined as the flow rate of the liquid divided by the cross-sectional area of the orifice), and  $\gamma$  is the value of interfacial tension between the monomer liquid or silicon oil and aqueous phases. We also determined the Reynolds number as  $Re = \rho Q/\eta h$  where  $\rho$  and  $Q$  are the density and the volume flow rate of the liquid, respectively, and  $h$  is the height of the channel (Anna et al. 2003). Later in the text we used  $Ca_o$ ,  $Ca_i$ ,  $Re_o$ , and  $Re_i$  where subscripts “o” and “i” correspond to the continuous phase and dispersed phases, respectively.

The volume,  $V$ , of an undeformed, spherical droplet was calculated as  $V = (4/3)\pi(D/2)^3$  where  $D$  is the droplet diameter. Droplets with a discoid shape formed when the diameter of an undeformed droplet was larger than the channel height,  $h$ . The volume of discoid droplets was approximated as  $V = (\pi/12)[2D^3 - (D-h)^2(2D + h)]$  (see Appendix).

### 3 Results

#### 3.1 Qualitative observations

Depending on the flow rates of the two immiscible liquids and on the properties of the dispersed (inner) phase, emulsification occurred in two different modes (see Fig. 2): (1) a dripping and (2) a jetting mode. In the dripping regime the thread of the inner phase broke either in the orifice, or in the close proximity of the orifice. In the jetting regime a continuous thread of the inner phase extended into the outlet channel and broke far (several widths of the orifice) downstream of the orifice. Because dripping in the confined geometry of the MFFD is strongly influenced by the geometry of the channels, this mode has different sub-modes of operation. Here we distinguish mode R1 (present at lower rates of flow of the inner phase) in which the thread broke in the orifice, and after each break-up the tip of the discontinuous stream retracted upstream of the orifice, to the end of its inlet channel. In the R1 mode the thread typically occupied most of the cross-section of the orifice. At higher rates of flow of the inner phase (mode R2), the break-up occurred either in the orifice, or slightly upstream of it, but the tip of the discontinuous stream did not retract to its inlet, but stayed at the inlet to the orifice and immediately reentered it for a successive break-up. In R2, the thread of the inner phase did not always occupy the entirety of the cross-section of the orifice and at higher rates of flow was focused in the orifice by the flow of the continuous fluid.

We know from our experiments with different geometries of the flow-focusing region (defined by the width of the inlet for the inner phase, the distance between the end of the inlet for the inner phase and the orifice, the width of the orifice, and the height of the channels) that these different modes of dripping can be tuned rationally. For example, increasing the ratio of the width of the inlet for the inlet phase to the distance between this inlet and the orifice suppresses the R1 mode. Although we do not report these observations here, it is also interesting to note that the transition between R1 and R2 often (e.g., in gas–liquid

systems) exhibits higher mode behaviors, like period 2 or period 4 dripping (Garstecki et al. 2004).

Each of the regimes described in the present work—the dripping (including R1 and R2) and the jetting modes—differed in the resulting characteristic variation in droplet sizes and polydispersity. Figure 2 and Table 2 summarize the qualitative features of the emulsification regimes at a constant flow rate ratio  $Q_o/Q_i$ . At low values of  $Q_o$ , and  $Q_i$ , (dripping, R1, Fig. 2a) the droplets were typically larger than the width of the orifice. In most cases, the diameter of droplets was also greater than the height of the downstream channel so they were squeezed between the top and bottom walls of the channel and acquired a discoid—rather than spherical—shape. Typically, the droplets produced in R1 had  $CV \leq 3.0\%$ . At moderate values of  $Q_o$ , and  $Q_i$ , (dripping, R2, Fig. 2b) droplets were monodisperse, with  $CV \leq 5\%$ ; however, in a narrow window of rates of flow of the droplet phase small satellite droplets were produced. At high values of  $Q_o$ , and  $Q_i$ , (jetting) the tip of the monomer liquid no longer retracted upstream of the orifice after break-up: instead, the stream of the dispersed fluid formed a “jet” that extended several hundreds of micrometers downstream of the orifice (Fig. 2c). We observed an abrupt increase of the length of the inner thread upon the transition from dripping to jetting. This jet was unstable with respect to the Rayleigh-Plateau instability and broke up into droplets (Probstein 1989). The droplets produced in this regime had dimensions significantly smaller than the width of orifice, with CV from 1.5 to 8%. The higher polydispersities occurred when secondary or satellite droplets accompanied the formation of the main population of droplets.

#### 3.2 Effect of viscosity of the droplet phase on the formation of droplets

We examined the effect of viscosity of the dispersed phase on droplet formation by emulsifying silicone oils with viscosities 10, 20, 50, 100, and 500 cP (the values of interfacial tension varied from 3.3 to 4.9 mN/m). Figure 3 illustrates the effect of the variation in the value of  $Q_o/Q_i$

**Fig. 2** Snapshots of different stages of the evolution of TPGDA droplets,  $Q_o/Q_i = 50$ . **a** Dripping regime—mode 1 (R1):  $Q_o = 0.02$  ml/h,  $Re_o = 0.065$ ,  $Re_i = 9.2 \times 10^{-5}$ . **b** Dripping regime—mode 2 (R2):  $Q_o = 0.25$  ml/h,  $Re_o = 0.81$ ,  $Re_i = 1.1 \times 10^{-3}$ . **c** Jetting regime:  $Q_o = 6.0$  ml/h,  $Re_o = 19.5$ ,  $Re_i = 0.028$ . Scale bar is 100  $\mu\text{m}$

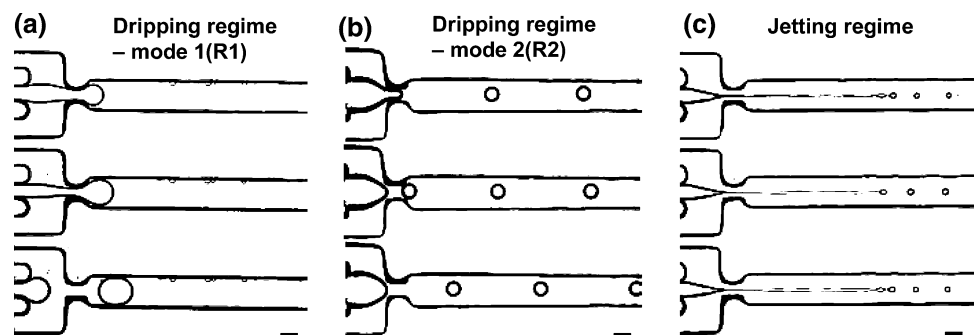


**Table 2** Three major regimes of droplet formation

Significant features	Dripping regime—mode 1 ( <i>R1</i> )	Dripping regime—mode 2 ( <i>R2</i> )	Jetting regime
Flow rates	Low $Q_o$ and $Q_i$	Moderate $Q_o$ and $Q_i$	High $Q_o$ and $Q_i$
Breakup point	<i>Inside</i> the orifice	<i>Inside</i> or <i>behind</i> but close to the orifice	<i>Behind and far away</i> the orifice
Size distribution	Narrow, CV < 3%	Depends on viscosity of droplet phase. In a particular window of flow rates CV < 1.8–2%;	In a particular window of flow rates 1.5 < CV < 8%. Droplets with broad size distribution can be formed
Droplet size and shape	Much larger than the orifice width; discoid shape	Comparable to the orifice width; discoid or spherical shape	Comparable or smaller than the orifice width; spherical shape

on the volume of the droplets (Fig. 3a–e), and representative micrographs of the system (Fig. 3a'–e'). In these experiments, we kept the rate of flow of the inner phase ( $Q_i$ ) constant. Monitoring the change of the volume of the droplets upon increase of the ratio of the rates of flow ( $Q_o/Q_i$ ) allowed us to determine the dominant mode of break-up. The rate-of-flow-controlled break-up (Garstecki et al. 2005c) predicts that the volume of the droplets is inversely proportional to ratio of the rates of flow:  $V_d \propto (Q_o/Q_i)^{-1}$ . The shearing mechanism relates the diameter of the droplet to the reciprocal of the capillary number, which yields a much stronger dependence on the ratio of the rates of flow  $V_d \propto (Q_o/Q_i)^{-3}$ .

Figure 3a–e shows that increasing the ratio ( $Q_o/Q_i$ ) of the flow rates of liquids resulted in a decrease of the volume of droplets. The decrease was approximately linear in ( $Q_o/Q_i$ ) for the low viscosity silicone oils, while it was much less significant for higher viscosity oils. These results suggest that the low viscosity fluids (e.g., silicon oil with viscosity 10 cP at ( $Q_o/Q_i$ ) ≤ 70, so that the viscosity contrast calculated as the ratio of the viscosity of the droplet phase to the viscosity of the continuous phase was lower than 20) followed the rate-of-flow-controlled break-up law [ $V_d \propto (Q_o/Q_i)^{-1}$ ], while fluids with high viscosity departed from the rate-of-flow mechanism, that is, the larger the viscosity, the smaller the dependence of droplet volume on the ratio of the rates of flow.

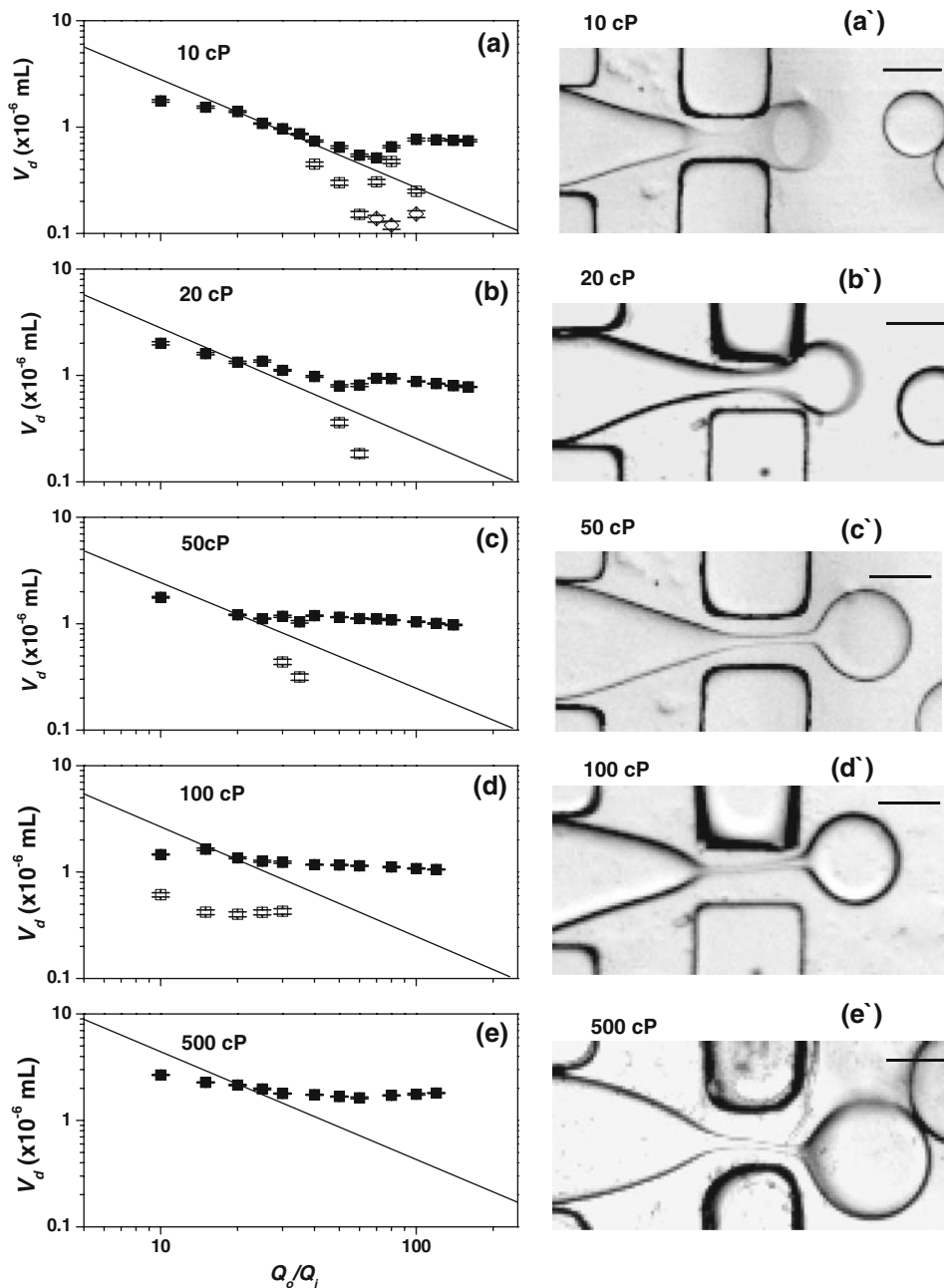
Inspection of the micrographs allowed us to postulate the possible mechanism behind the divergence of the break-up dynamics from the rate-of-flow mechanism at high values of the viscosity of the inner fluid. Since in the dripping regime the thread of the inner phase blocks most of the cross-section of the orifice, there is the build-up of pressure required for the rate-of-flow mechanism to ensue. This build up of pressure in the continuous phase squeezes the inner thread (the neck between the stream of the inner phase and the emerging droplet) and, at the same time,

pushes the emerging droplet out of the orifice. Because for high viscosity liquids the surface tension-driven collapse of the neck at the late stage of the pressure-driven break-up is slow [as at the very last stage of break-up it is surface tension driven and proceeds at the capillary speed  $u_{ca} \sim O(\mu/\gamma)$ ] versus closed symbols the droplet is pushed outside of the orifice before the neck collapses. As a result, the break-up takes longer and the droplets are larger than in the case of low viscosity fluids, for which the time of break-up is defined only by the volume of the orifice and the rate of flow of the outer phase.

We note that for fluids with low viscosity the breakup dynamics departed from this response at high values of  $Q_o/Q_i$ , where the drop volume no longer changed significantly with the rate of flow. For fluids with higher viscosity this departure occurred at lower flow rate ratios, e.g. at  $Q_o/Q_i = 70$  for silicon oil with  $\eta_i = 10$  cP and  $Q_o/Q_i = 50$  for silicon oil with  $\eta_i = 20$  cP. Moreover, at the same flow rate ratios, highly viscous silicon oil produced larger droplets (Fig. 3a–e): e.g., for  $Q_o/Q_i = 50$  silicone oil with viscosity 500 cP produced droplets ca. 50% larger than silicon oil with viscosity 10 cP. For silicone oils with viscosity from 10 to 100 cP, a range of values of  $Q_o/Q_i$  existed, in which droplets with bimodal or trimodal distribution were generated (e.g. open vs. closed symbols in Fig. 3b–d). By contrast, a highly viscous silicone oil with  $\eta_i = 500$  cP formed monodisperse droplets with CV ≈ 2% over the entire range of  $Q_o/Q_i$ .

In Fig. 4 we plot the results of similar experiments to the ones described above, but conducted with the three monomer liquids (DVB, TPGDA, and MAOP-DMS). These monomers behave similarly to the silicone oils, following approximately the rate-of-flow-controlled break-up mechanism, with a strong departure from it at the transition to jetting. Figure 4 a–c shows the dependence of the volume of droplets on the variation in ratio  $Q_o/Q_i$  (for  $Q_i = 0.01$  ml/h). Two common features were observed for

**Fig. 3** A log–log variation in the droplet volume,  $V_d$  of silicon oil with different viscosity plotted as a function of water-to-oil flow rate ratio,  $Q_o/Q_i$ , at constant silicon oil flow rate 0.04 ml/h for  $2.6 \times 10^{-4} \leq Re_i \leq 0.13$ ;  $1.3 \leq Re_o \leq 26$ . Snapshots of droplets formed from silicone oil with different viscosity under the same hydrodynamic conditions ( $Q_o/Q_i = 20$ ,  $Q_i = 0.04$  ml/h). In **a–e** primary droplets (filled square), secondary droplets (open square, open diamond). **a** 10 cP. **b** 20 cP. **c** 50 cP. **d** 100 cP. **e** 500 cP. Scale bar in **a'–e'** is 100  $\mu\text{m}$ . The solid line is given for visual guidance



all monomers: (1) the decreasing size of droplets when the ratio  $Q_o/Q_i$  increased and (2) the stabilized size of droplets for  $Q_o/Q_i > 150$ . In summary, we found that viscosity of the inner phase has a pronounced effect both on the type of the scaling of the size of the droplets with the rates of flow of the liquids, and on the dimensions of the droplets.

Moderately viscous TPGDA (14 cP) formed highly monodisperse droplets with  $1.5\% < CV < 3.0\%$  in the entire range of the ratios  $Q_o/Q_i$  whereas MAOP-DMS (20 cP) and DVB (1 cP) formed monodisperse droplets only in a particular window of the values of  $Q_o/Q_i$  ( $Q_o/Q_i < 55$  and  $Q_o/Q_i < 100$ , respectively). Outside these

windows, emulsification of MAOP-DMS and DVB produced several populations of droplets with different sizes: in each cycle after releasing a primary droplet, the liquid thread broke again once or twice, releasing secondary and tertiary droplets, respectively. The diameters of multiple droplets produced in each series were from 20 to 170  $\mu\text{m}$ . Although the generation of multiple populations of droplets resulted in the overall broad size distribution of droplets, each population of droplets had a relatively narrow size distribution of ca.  $CV < 5\%$  for MAOP-DMS and  $CV < 9.5\%$  for DVB. We stress a striking difference (e.g. exemplified by the formation of secondary droplets)

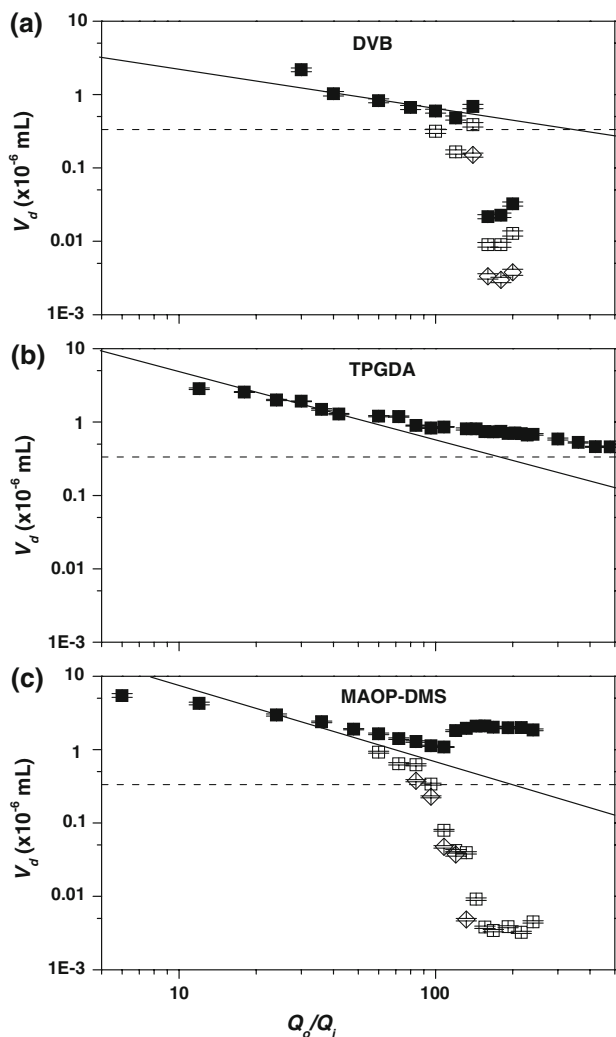


**Fig. 4** A log–log variation in the droplet volume,  $V_d$  of DVB (a), TPGDA (b) and MAOP-DMS (c) plotted versus water-to-oil flow rate ratio,  $Q_o/Q_i$ , at constant monomer flow rate,  $Q_i = 0.01$  ml/h.  $1.7 \times 10^{-3} \leq Re_i \leq 0.032$ ; The horizontal dashed lines in (a–c) indicate the transition from the formation of spherical droplets (below) to discoid droplets (above). In (a–c) primary droplets (filled square), secondary droplets (open square, open diamond). The solid line is given for visual guidance

between the emulsification of TPGDA and MAOP-DMS, the liquids that showed close values of interfacial tension with the continuous phase but approximately 40% difference in viscosities.

**4 Discussion**

**4.1 Volume of the droplets**

To relate the size of droplets to the properties and the flow rates of liquids, we summarized the results of our experiments in Figs. 5 and 6. Figure 5 summarizes the variation

in dimensionless droplet volume  $V = V_d/V_c$ , where  $V_d$  is the volume of the droplet, and  $V_c$ , is the cube of the width of the orifice, with the flow rate of continuous phase ( $Q_o$ ) at a constant rate of flow of the droplet phase ( $Q_i = 0.04$  mL/h) for all the fluids that we used in our study. This plot clearly excludes the dominant role of shear in the process of break-up. A shearing model for break-up in unbounded fluids would predict  $V \propto Q_o^{-3}$ . The effects of confinement can modify the exponent, yet, for the shear induced break-up we expect a strong dependence of  $V$  on the flow of the outer fluid (proportional to  $Q_o$ ). In Fig. 5, we see that for all the fluids the exponent  $\alpha$  in  $V \propto Q_o^\alpha$  is less than unity. As we discussed in the previous section this data suggests that low viscosity fluids break up according to the rate-of-flow-controlled mechanism (Garstecki et al. 2005c), while the fluids of higher viscosity gradually depart from this model, showing gradually weaker dependence of the volume of droplets on the rates of flow of the continuous (outer) fluid.

In order to further examine the role of the capillary number in the process of break-up we conducted experiments in which the ratio of the rates of flow ( $Q_o/Q_i$ ) was held constant, while we increased the two rates of flow simultaneously at a constant proportion of  $Q_o/Q_i = 60$ . In Fig. 6 we plotted the dimensionless volume of droplet,  $V_d/V_c$ , as a function of the capillary number  $Ca_o$  of the continuous phase. We verified that the Weber number,  $We = \rho v^2 l / \gamma$ , was approximately 0.0015~0.40; since  $We < 1$  the interfacial tension forces dominate inertia and the capillary number forms the correct dimensionless group

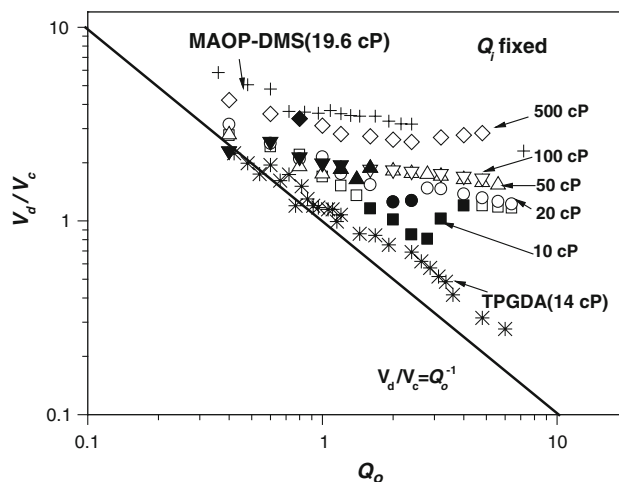


**Fig. 5** A log–log plot of the variation in the dimensionless droplet volume,  $V_d/V_c$  (defined as droplet volume  $V_d$  divided by the cube of orifice width  $V_c$ ) of dispersed phase plotted as a function of water flow rate,  $Q_o$ , for constant flow rate 0.04 ml/h of the droplet phase: star TPGDA, plus MAOP-DMS, and silicone oil with different viscosity, cP: open square 10, open circle 20, open triangle 50, inverted open triangle 100, open diamond 500. Corresponding solid symbols presents volume of primary droplets accompanied with secondary or satellite droplets. The solid line is given for visual guidance

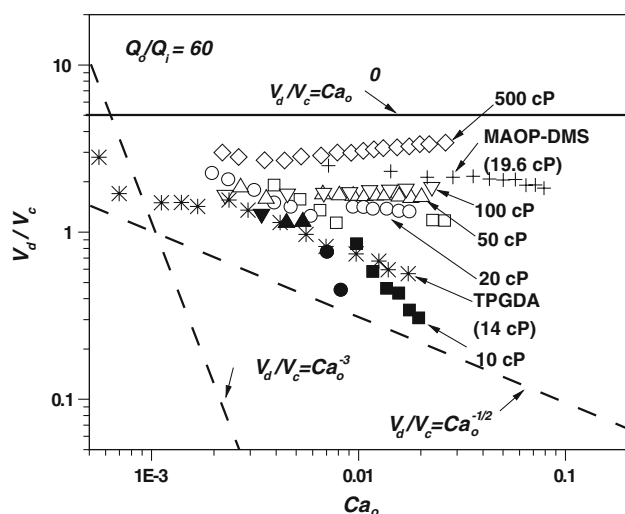


**Fig. 6** A log–log variation in the dimensionless droplet volume,  $V_d/V_c$  plotted as a function of capillary number  $Ca_o$  of the continuous phase, for constant water-to-monomer flow rate ratio  $Q_o/Q_i = 60$  for  $3.2 \times 10^{-5} \leq Re_i \leq 0.16$ ;  $0.96 \leq Re_o \leq 9.6$  for monomers: *star* TPGDA, *plus* MAOP-DMS and *times* DVB and silicone oil with different viscosity, cP: *open square* 10, *open circle* 20, *open triangle* 50, *inverted triangle* 100, *open diamond* 500. Corresponding solid symbols presents volume of primary droplets accompanied with secondary or satellite droplets. The *straight solid* and *dash lines* are given for visual guidance

for the description of the behavior of our system. We note that the capillary numbers of the droplet and continuous phase,  $Ca_i$  and  $Ca_o$ , respectively, are related as  $Ca_i = Ca_o(Q_i\eta_i/Q_o\eta_o)$  (Serra et al. 2007).

For this experiment, the rate-of-flow-controlled break-up model predicts no variation in the volume of the droplets (since the value of  $Q_o/Q_i$  stays constant), while the shearing mechanism predicts the volume to decrease with the capillary number (with the third power of  $Ca$  for break-up in unbounded fluids). Figure 6 shows that the dependence on  $Ca$  is much weaker and thus it is difficult to associate the break-up process with a simple competition between the shear stress exerted on the emerging droplet by the continuous phase and the interfacial stresses (Zhang and Stone 1997; Zhang 1999). The weak dependence of droplet volume on the capillary number excludes the dominant role of the rate-of-flow mechanism in the dynamics of break-up and—for the viscosities that we tested—stays within  $V \propto (Q_o/Q_i)^{-1/2}$  and  $V \propto (Q_o/Q_i)^0$ , with the larger viscosity fluids showing a weaker dependence of  $V$  on  $Ca$ . A similar weak dependence of the size of the droplets on the value of the capillary number has also been observed for the break-up at T-junctions operating at low values of  $Ca$  (De Menech et al. 2007). Nonetheless, our results suggest a rate-of-flow-controlled break-up for fluids with low viscosities, as reported earlier for the formation of bubbles in flow-focusing geometries (Garstecki et al. 2005c), with other effects, including the retardation of

the speed of break-up by a high viscosity of the fluids and possible viscoelastic effects. It is also possible that to explain the variability in experiments with similar viscosity ratios that gradients of the concentration of surfactant on the interface (Liao et al. 2006) impact the dynamics of the drop formation process.

## 4.2 Size distribution

Our work shows that for all liquids studied in the present work emulsification conducted in MFFDs is an efficient method for the production of droplets with a narrow size distribution. The regimes of formation of monomer and oil droplets were similar to those observed earlier for the aqueous droplets emulsified in an organic continuous phase (Anna et al. 2003). Here however we show that the type and the number of regimes of emulsification depend on the viscosity of the droplet phase. For every system used in the present study, we found the range of flow rates and the flow rate ratios of the two immiscible liquids within which a single population of droplets with narrow polydispersity was formed. The range of polydispersity broadened for liquids with lower viscosities.

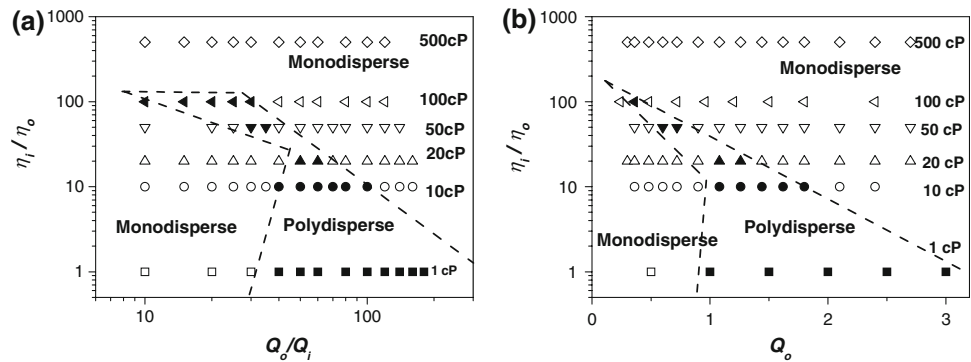
Figure 7a maps the behavior of the system onto the  $(\eta_i/\eta_o, Q_o/Q_i)$  space, where  $\eta_i/\eta_o$  is the viscosity contrast defined as the ratio of the viscosity of the dispersed phase to the viscosity of the aqueous (continuous) phase ( $\eta_o = 1$  cP). This diagram outlines the regions of the generation of a single population of monodisperse droplets. Liquids with higher viscosity featured a broader window of the ratios of rates of flow, generating droplets with a narrow size distribution. In Fig. 7b we map the behavior of the system for different values of the ratio of viscosity ( $\eta_i/\eta_o$ ) and a range of the rates of flow of the continuous fluid. This diagram shows that an increase of the viscosity of the droplet phase resulted in broadening of the range of rates of flow in which monodisperse droplets were obtained.

## 5 Conclusions

Our study shows that for a wide range of liquids with different viscosities emulsification in microfluidic flow-focusing devices is an efficient method for the production of nearly monodisperse emulsions. For a particular geometry and surface energy of the MFFD and a constant viscosity of the continuous phase, the *only* parameters that determine the behavior of the system are: (1) the rates of flow of the droplet and continuous phases, and (2) the macroscopic properties of liquids. Viscosity played an important role in the emulsification, as well as the dynamics of the breakup of droplets. We found it impossible to predict the variation in the size of the droplets of *various* liquids as a function of the  $Ca$  alone. Our results



**Fig. 7** “Phase-like” diagram of the generation of the droplets in the  $(\eta_i/\eta_o, Q_o/Q_i)$  space at  $Q_i = 0.04$  ml/h (a) and in the  $(\eta_i/\eta_o, Q_o)$  space at constant flow rate ratio,  $Q_o/Q_i = 60$  (b): empty and filled symbols show the regions of production of monodisperse and polydisperse droplets, respectively. Dashed lines are given for visual guidance for the transitions between different regions

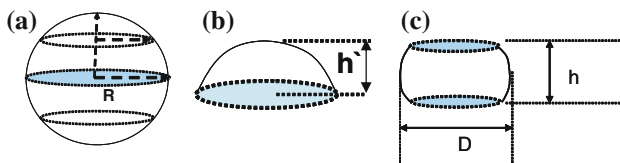


suggest, nonetheless, for fluids with low viscosities, a mechanism of break-up that is controlled by the rate of flow of the fluids. The results presented in this study should facilitate the selection of liquids based on their macroscopic properties and flow parameters for the controlled formation of highly monodisperse droplets.

**Acknowledgments** This work was supported by the US Department of Energy under award DE-FG02-00ER45852 and Canada Research Chair Grant. P.G. acknowledges financial support from the Foundation for Polish Science and the support from the Ministry of Science and Higher Education of Poland for the years 2006–2009. We thank for Prof. David James and Ryan Grau (University of Toronto) for helping us in rheology experiments.

**Appendix**

The volume of an undeformed spherical droplet is given by  $V = 4/3 \pi R^3$  where  $R$  is the radius of the droplet. The volume of the droplet segment is given by  $V_s = 1/3 \pi h^2 (3R - h')$  where  $h$  is the height of the segment. The volume of the disk with height  $h$  ( $h = 2R - h'$ ) is thus equal to  $(\pi/12)[2D^3 - (D - h)^2 (2D + h)]$  where  $D$  is the diameter of the disk.



**References**

Anna SL, Bontoux N, Stone HA (2003) Formation of dispersions using “flow-focusing” in microchannels. *Appl Phys Lett* 82: 364–363  
 Christopher GF, Anna SL (2007) Microfluidic methods for generating continuous droplet streams. *J Phys D App Phys* 40:R319–R336  
 Cohen I, Li H, Hougland JL, Mrksich M, Nagel SR (2001) Using selective withdrawal to coat microparticles. *Science* 292:265–267  
 Cramer C, Fischer P, Windhab EJ (2004) Drop formation in a co-flowing ambient fluid. *Chem Eng Sci* 59:3045–3058

Cygan ZT, Cabral JT, Beers KL, Amis EJ (2005) Microfluidic platform for the generation of organic-phase microreactors. *Langmuir* 21:3629–3634  
 De Menech M, Garstecki P, Jousse F, Stone HA (2007) Transition from squeezing to dripping in a microfluidic T-shaped junction. *J Fluid Mech* 595:141–162  
 Dendukuri D, Tsoi K, Hatton TA, Doyle PS (2005) Controlled synthesis of nonspherical microparticles using microfluidics. *Langmuir* 21:2113–2116  
 Dreyfus R, Tabeling P, Willaime H (2003) Ordered and disordered patterns in two-phase flows in microchannels. *Phys Rev Lett* 90:144505/1–144505/4  
 El-Ali J, Gaudet S, Gunther A, Sorger PK, Jensen KF (2005) Cell stimulus and lysis in a microfluidic device with segmented gas–liquid flow. *Anal Chem* 77:3629–3636  
 Freer EM, Wong H, Radke CJ (2005) Oscillating drop/bubble tensiometry: effect of viscous forces on the measurement of interfacial tension. *J Colloid Interface Sci* 282:128–132  
 Ganan-Calvo AM (1998) Generation of steady liquid microthreads and micron-sized monodisperse sprays in gas streams. *Phys Rev Lett* 80:285–288  
 Ganan-Calvo AM, Gordillo JM (2001) Perfectly monodisperse microbubbling by capillary flow focusing. *Phys Rev Lett* 87: 274501  
 Garstecki P, Gitlin I, DiLuzio W, Whitesides GM, Kumacheva E, Stone HA (2004) Formation of monodisperse bubbles in a microfluidic flow-focusing device. *Appl Phys Lett* 85:2649–2651  
 Garstecki P, Fischbach MA, Whitesides GM (2005a) Design for mixing using bubbles in branched microfluidic channels. *Appl Phys Lett* 86:244108  
 Garstecki P, Fuerstman MJ, Whitesides GM (2005b) Nonlinear dynamics of a flow-focusing bubble generator: an inverted dripping faucet. *Phys Rev Lett* 94:234502/1–234502/4  
 Garstecki P, Stone HA, Whitesides GM (2005c) Mechanism for flow-rate controlled breakup in confined geometries: a route to monodisperse emulsions. *Phys Rev Lett* 94:164501  
 Garstecki P, Fuerstman MJ, Stone HA, Whitesides GM (2006) Formation of droplets and bubbles in a microfluidic T-junction - scaling and mechanism of break-up. *Lab Chip* 6:437–446  
 Guillot P, Colin A (2005) Stability of parallel flows in a microchannel after a T junction. *Phys Rev E* 72:066301  
 Hudson SD, Cabral JT, Goodrum WJ, Beers KL, Amis EJ (2005) Microfluidic interfacial tensiometry. *Appl Phys Lett* 87: 081905  
 Jensen K, Lee A (2004) The science and applications of droplets in microfluidic devices—Foreword. *Lab Chip* 4:31N–32N  
 Jeong WJ, Kim JY, Choo J, Lee EK, Han CS et al (2005) Continuous fabrication of biocatalyst immobilized microparticles using photopolymerization and immiscible liquids in microfluidic systems. *Langmuir* 21:3738–3741

- Khan SA, Gunther A, Schmidt MA, Jensen KF (2004) Microfluidic synthesis of colloidal silica. *Langmuir* 20:8604–8611
- Lewis PC, Graham RR, Nie ZH, Xu SQ, Seo M, Kumacheva E (2005) Continuous synthesis of copolymer particles in microfluidic reactors. *Macromolecules* 38:4536–4538
- Li W, Nie ZH, Zhang H, Paquet C, Seo M, Garstecki P, Kumacheva E (2007) Screening of the effect of surface energy of microchannels on microfluidic emulsification. *Langmuir* 23:8010–8014
- Liao YC, Franses EI, Basaran OA (2006) Deformation and breakup of a stretching liquid bridge covered with an insoluble surfactant monolayer. *Phys Fluids* 18:022101
- Link DR, Anna SL, Weitz DA, Stone HA (2004) Geometrically mediated breakup of drops in microfluidic devices. *Phys Rev Lett* 92:054503
- Loscerales IG, Barrero A, Guerrero I, Cortijo R, Marquez M, Ganan-Calvo AM (2002) Micro/nano encapsulation via electrified coaxial liquid jets. *Science* 295:1695–1698
- Nie ZH, Li W, Seo M, Xu SQ, Kumacheva E (2006) Janus and ternary particles generated by microfluidic synthesis: Design, synthesis, and self-assembly. *J Am Chem Soc* 128:9408–9412
- Nie ZH, Xu SQ, Seo M, Lewis PC, Kumacheva E (2005) Polymer particles with various shapes and morphologies produced in continuous microfluidic reactors. *J Am Chem Soc* 127:8058–8063
- Nisisako T, Torii T, Higuchi T (2002) Droplet formation in a microchannel network. *Lab Chip* 2:24–26
- Nisisako T, Torii T, Higuchi T (2004) Novel microreactors for functional polymer beads. *Chem Eng Sci* 101:23–29
- Probstein RF. (1989) *Physicochemical hydrodynamics: an introduction*. Butterworth Publishers, London
- Seo M, Nie ZH, Xu SQ, Lewis PC, Kumacheva E (2005a) Microfluidics: From dynamic lattices to periodic arrays of polymer disks. *Langmuir* 21:4773–4775
- Seo M, Nie ZH, Xu SQ, Mok M, Lewis PC et al (2005b) Continuous microfluidic reactors for polymer particles. *Langmuir* 21:11614–11622
- Serra C, Berton N, Bouquery M, Prat L, Hadziioannou G (2007) A predictive approach of the influence of the operating parameters on the size of polymer particles synthesized in a simplified microfluidic system. *Langmuir* 23:7745–7750
- Song H, Tice JD, Ismagilov RF (2003) A microfluidic system for controlling reaction networks in time. *Angew Chem Int Ed Engl* 42:768–772
- Sugiura S, Nakajima M, Ito H, Seki M (2001) Synthesis of polymeric microspheres with narrow size distributions employing microchannel emulsification. *Macromol Rapid Commun* 22:773–778
- Sugiura S, Nakajima M, Seki M (2002a) Effect of channel structure on microchannel emulsification. *Langmuir* 18:5708–5712
- Sugiura S, Nakajima M, Seki M (2002b) Prediction of droplet diameter for microchannel emulsification. *Langmuir* 18:3854–3859
- Takeuchi S, Garstecki P, Weibel DB, Whitesides GM (2005) An axisymmetric flow-focusing microfluidic device. *Adv Mater* 17:1067–1072
- Tan YC, Cristini V, Lee AP (2006) Monodispersed microfluidic droplet generation by shear focusing microfluidic device. *Sens Actuators B* 114:350–356
- Thorsen T, Roberts RW, Arnold FH, Quake SR (2001) Dynamic pattern formation in a vesicle-generating microfluidic device. *Phys Rev Lett* 86:4163–4166
- Tice JD, Song H, Lyon AD, Ismagilov RF (2003) Formation of droplets and mixing in multiphase microfluidics at low values of the Reynolds and the capillary numbers. *Langmuir* 19:9127–9133
- Utada AS, Lorenceau E, Link DR, Kaplan PD, Stone HA, Weitz DA (2005) Monodisperse double emulsions generated from a microcapillary device. *Science* 308:537–541
- Ward T, Faivre M, Abkarian M, Stone HA (2005) Microfluidic flow focusing: Drop size and scaling in pressure versus flow-rate-driven pumping. *Electrophoresis* 26:3716–3724
- Xia YN, Whitesides GM (1998) Soft lithography. *Angew Chem Int Ed Engl* 37:551–575
- Xu QY, Nakajima M (2004) The generation of highly monodisperse droplets through the breakup of hydrodynamically focused microthread in a microfluidic device. *Appl Phys Lett* 85:3726–3728
- Xu SQ, Nie ZH, Seo M, Lewis P, Kumacheva E et al (2005) Generation of monodisperse particles by using microfluidics: Control over size, shape, and composition. *Angew Chem Int Ed Engl* 44:724–728
- Zhang DF, Stone HA (1997) Drop formation in viscous flows at a vertical capillary tube. *Phys Fluids* 9:2234–2242
- Zhang H, Tumarkin E, Peerani R, Nie Z, Sullan RMA et al (2006) Microfluidic production of biopolymer microcapsules with controlled morphology. *J Am Chem Soc* 128:12205–12210
- Zhang XG (1999) Dynamics of drop formation in viscous flows. *Chem Eng Sci* 54:1759–1774
- Zheng B, Ismagilov RF (2005) A microfluidic approach for screening submicroliter volumes against multiple reagents by using preformed arrays of nanoliter plugs in a three-phase liquid/liquid/gas flow. *Angew Chem Int Ed Engl* 44:2520–2523
- Zheng B, Roach LS, Ismagilov RF (2003) Screening of protein crystallization conditions on a microfluidic chip using nanoliter-size droplets. *J Am Chem Soc* 125:11170–11171